Clays and Clay Minerals, Vol. 54, No. 5, 571–586, 2006.

THE SMECTITE-TO-DISORDERED KAOLINITE TRANSITION IN A TROPICAL SOIL CHRONOSEQUENCE, PACIFIC COAST, COSTA RICA

G. Burch Fisher† and Peter C. Ryan*

Geology Department, Middlebury College, Middlebury, VT, 05753 USA

Abstract—Soils developed on Quaternary fluvial fill terraces in the humid tropics of Costa Rica display progressive changes in mineral assemblage, chemical composition and particle size with age. Clay minerals from B horizons of active floodplains are predominantly smectite with lesser amounts of disordered kaolinite. B horizons in 5 to 10 ka soils consist of sub-equal amounts of smectite and disordered kaolinite, and soils on 37–125 ka terraces consist of disordered kaolinite with only traces of smectite. The composition of the smectite, as determined by EDX scans of smectite-rich pore space, is $[(Mg_{0.2},Ca_{0.1})(Fe_{0.6}Al_{1.4})(Si_{3.6}Al_{0.4})O_{10}(OH)_2]$, consistent with ferruginous beidellite.

Bulk mineral assemblage varies from a smectite-plagioclase-augite-quartz-magnetite assemblage in $\leqslant$10 ka terrace soils to a disordered kaolinite-goethite-hematite-quartz-magnetite assemblage in $\geqslant$37 ka terrace soils. Leaching results in rapid loss of soluble base cations and residual concentration of Ti and Zr indicates mass losses of ~50% by chemical denudation by 125 ka. Plots of terrace age *vs*. various measures of clay mineralogy, chemical composition, and particle size produce parabolic curves consistent with rapid chemical weathering pre-37 ka and slower to imperceptible rates of change from 37 to 125 ka. For some pedogenic properties, particularly particle size and concentrations of base cations and Zr, soils appear to reach steady-state conditions within 37 ka.

These results were applied to interpretation of landscape evolution in this tectonically active region by: (1) facilitating identification of two Holocene (5 ka and 10 ka) terraces on the Esterillos Block 5–30 m above sea level (masl), and two Pleistocene terraces $\geqslant$125 ka on the Parrita Block 30 masl, and, in turn, (2) documenting uplift rates as high as 4.4 m/ka between 37 and 10 ka on the Esterillos Block, and as low as 0.1 m/ka over the past 125 ka on the adjacent Parrita Block. These findings are consistent with previous work indicating that the subduction of anomalous bathymetric features at the Middle America Trench is having a significant impact on fore-arc dynamics and topography over relatively short geological time periods and spatial scales.

Key Words—Beidellite, Costa Rica, Disordered Kaolinite, Geochemistry, Halloysite, Mineralogy, Smectite, Soil, Steady State, Terraces, Tropical.

INTRODUCTION

Intense leaching in humid tropical climates typically produces soils depleted in base cations and Si and enriched in the more immobile elements such as Fe, Al, Ti and Zr (White *et al.*, 1998), and consequently pedogenesis in the tropics plays an important role in the transport of dissolved ions to oceans (*e.g.* 65% of dissolved marine silica is derived from tropical soils; Meybeck, 1987) and in CO_2 cycling. These soils are commonly dominated by relatively stable assemblages of halloysite or kaolinite and hydroxides and oxides of Al and Fe with low cation exchange capacities. In spite of extensive knowledge of weathering in humid tropical environments, two important issues that remain unresolved are (1) the rate at which soil pedogenesis occurs on a trajectory toward steady state, and (2) the underlying cause of the multiple pathways by which pedogenic kaolin forms – for example, the following trends have been documented in tropical soils:

10 Å halloysite → 7 Å halloysite (Nieuwenhuyse and van Breeman, 1997; Kautz and Ryan, 2003);

halloysite → disordered kaolinite → kaolinite (Hughes, 1980);

kaolinite → halloysite (Singh and Gilkes, 1992);

smectite → halloysite or kaolinite *via* interstratified kaolinite-smectite (K-S – Herbillon *et al.*, 1981; Yerima *et al.*, 1985; Muhs, 2001) or halloysite-smectite (H-S – Delvaux *et al.*, 1990);

allophane and other short-range order aluminosilicates → kaolin (Nieuwenhuyse and van Breemen, 1997).

Note that all examples result in end-member kaolin minerals, but that the processes and pathways are variable. As far as we know, no study has observed direct transformation of smectite → kaolin (*i.e.* without intermediary K-S or H-S) in tropical soils. Given the wide range in physico-chemical properties of the above-mentioned soil clays (particularly cation exchange capacity), understanding reaction pathways and kinetics is important in the analysis of tropical soils.

Terraces are some of the best examples in the geological record of soil chronosequences (Birkeland,

* E-mail address of corresponding author:
pryan@middlebury.edu
†Current Address: Earth Sciences Department, Dartmouth College, Hanover, NH, 03755 USA
DOI: 10.1346/CCMN.2006.0540504

1999). They commonly contain information regarding the chronological nature of chemical weathering, particularly element depletion and enrichment trends and pedogenic mineral paragenesis (Merritts *et al.*, 1992; Vidic and Lobnik, 1997). Terrace sequences also commonly preserve information related to landscape evolution. For example, along the Pacific coast of Costa Rica, studies of fluvial terraces have helped to estimate uplift rates in the tectonically active Central American fore-arc (Figure 1; Fisher *et al.*, 1998).

This study seeks to address two main issues. The first is rates and pathways of chemical weathering, particularly geochemical depletion and enrichment, the transition of pedogenic smectite to kaolin, and the appearance of steady-state conditions in tropical soils. The second is the application of mineralogical and geochemical data to correlation of fluvial terraces across tectonic blocks undergoing differential uplift. We present an analysis of the geochemical and mineralogical evolution of soils in a tropical chronosequence where soil age ranges from mid Holocene (5 ka) to late Pleistocene (125 ka), and apply the results to regional fluvial terrace correlation.

STUDY AREA

The study area is located on the Esterillos and Parrita tectonic blocks along the central Pacific coast of Costa Rica near the town of Parrita (Figure 1). The field area encompasses the lower Rio Parrita watershed including terraces formed by Quaternary fill sediments between Parrita and Esterillos Este. Bedrock in the headwaters of the Parrita watershed is predominantly igneous extrusive rock (basalt and andesite); further downstream toward its confluence with the Pacific Ocean, exposed bedrock in the watershed is dominated by Cretaceous Nicoya Complex ophiolites (predominantly basalt and volcani-

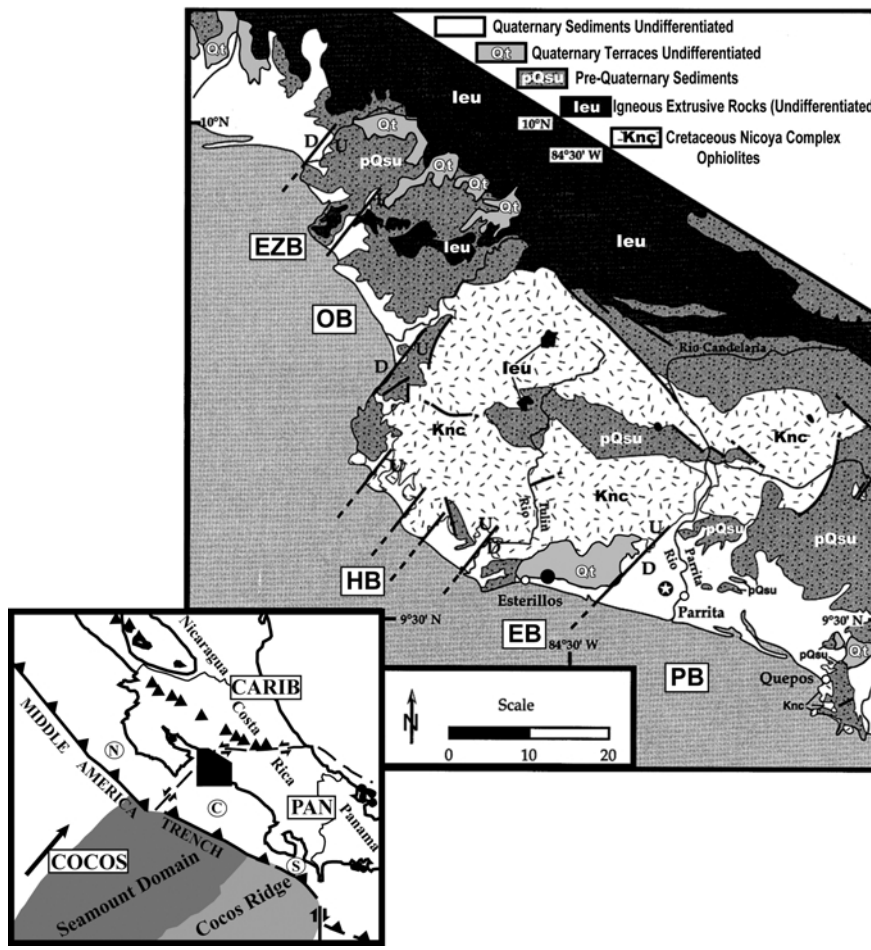

Figure 1. Simplified geological map of the central Pacific coast region modified from Sak *et al.* (2004a) with inset map showing the location of the Middle America Trench and relative Cocos plate motion (modified from Silver *et al.*, 2004). Fore-arc blocks are shown in boxes and bounded by significant fault margins. Uplift is continuous throughout the blocks but D/U symbols are indicative of differential uplift rates and relative block motions. PB = Parrita Block; EB = Esterillos Block; HB = Herradura Block; OB = Orotina Block. Symbols: white star: location of Finca Los Angeles weather station; ● location of dated woody debris at the base of Qt-2-1.

clastic sedimentary rock). The subduction of oceanic crust of differential thickness has created a system of active faults oriented at high angles to the subduction zone that segment the fore-arc thrust belt into blocks with contrasting uplift rates (Gardner *et al.*, 1992; Fisher *et al.*, 1998). Pacific slope fluvial systems generally follow these margin-perpendicular faults and their fluvial fill terraces can be used to infer differential uplift rates associated with each block (Pazzaglia *et al.*, 1998). Geochemical modeling of weathering of basalt clasts constrained by radiocarbon and Ar-Ar dating documents three prominent Pleistocene terraces that formed during high sea level stands at 37 ka (Qt-3; Oxygen Isotope Stage 3), 125 ka (Qt-2; OIS 5e), and 240 ka (Qt-1; OIS 7) (Sak *et al.*, 2004a). Quaternary sediments are present at elevations <250 m above sea level (masl) and terrace exposures are confined to the lower reaches of the river where the modern stream gradient is <3 m/km. All study sites were located on flat-topped terrace deposits (increasingly dissected with age) confined to elevations <210 masl.

Soils in the Parrita-Esterillos area have been mapped at the soil order scale and generally have been classified as Inceptisols (Harris *et al.*, 1971; www.eosl.eas.ualberta.ca/maps/costaricamaps.asp). Detailed climatic data are available from Finca Los Angeles (N9º30′W84º24′), a site near Parrita located ~5 masl (Figure 1). Mean annual temperature (MAT) and mean annual precipitation (MAP) for the period extending from 1941 to 1982 are 27.3ºC and 3085 mm, respectively (Sak *et al.*, 2004a). Temperature stays relatively constant, ranging from 26.5ºC in October to 28.5ºC in March. Precipitation, however, does fluctuate throughout the year with the majority falling between the months of July and November. The maximum amount of rain falls in October (570 mm) and the minimum in March (28.5 mm). Although the mineralogy and chemistry of soils along the Pacific slope of Costa Rica have not previously been studied beyond the weathering rind work of Sak *et al.* (2004a), northeast of the volcanic cordillera and 100 km north of the area studied here, Nieuwenhuyse and van Breeman (1997) and Kautz and Ryan (2003) described the mineralogical and chemical evolution of terrace soils in lowland rainforest on the low-lying Atlantic slope of Costa Rica, where MAT = 25ºC and MAP = 4000 mm. The dissolution of plagioclase and augite occurs rapidly, to the point that both comprise $\leqslant$1% of soils older than 10 ka. 10 Å halloysite is the dominant pedogenic mineral in soils <1 ka, whereas 7 Å halloysite is the dominant mineral in soils >10 ka. Smectite is only present in active floodplains (<1 ka), where it occurs in minor amounts as high-charge dioctahedral smectite. Rapid depletion of soluble base cations and residual concentration of Al, Fe, Ti and Zr indicate that these soils reach a steady state by 10 ka, where no significant difference in soil mineralogy or chemistry exists in soils ranging in age from 10 ka to 1.2 Ma.

MATERIALS AND METHODS

Seven fluvial fill terraces were sampled from the Rio Parrita basin (four on the Esterillos block and three on the adjacent Parrita block). Two sediment samples from the Rio Parrita 1−2 year floodplain (AS) were also obtained. Terraces sampled include sediments in the most recently formed terrace (Qt-5), which is exposed on both the Esterillos and Parrita blocks, an older recently formed terrace (Qt-4) on the Esterillos Block, the 37 ka (Qt-3) and 125 ka terraces (Qt-2) on the Esterillos Block, and a couple of low-elevation yet highly weathered terraces on the Parrita Block (Qt-P). The 240 ka Qt-1 terrace described by Sak *et al.* (2004a) is not present in the study area. Samples are labeled chronologically with the terrace identification (Qt-2) followed by terrace number (*e.g.* Qt-2-1; used in cases where more than one soil profile was sampled on a given terrace) and then the soil sample horizon (Qt-2-1-B2, denoting B2 horizon, soil profile 1, Qt-2 terrace) (Table 1). Terraces were sampled at 10 cm (B1), 20 cm (B2), and 1 m (B3) (except for AS samples, Qt-5-1, and Qt-5-2 sites). When road cuts provided deeper soil exposures (Qt-4, Qt-2-1), samples were taken every meter below B3 into the C horizon (C1, C2, *etc.*) at depths up to 8 m. (Detailed sample locations are available at http://community.middlebury.edu/~pryan). Profiles were described using standard procedures (Birkeland, 1999); B horizons were distinguished from C horizons in the field by distinct color transitions from dark red to yellowish-brown (these field-based observations were confirmed by mineralogical and geochemical data, presented in the Results section below). To avoid desiccation and mineral dehydration, samples were double-bagged immediately after sampling and XRD analyses were performed within 24 h of slide preparation. Sampling locations were identified using previously sampled and established terraces (Sak *et al.*, 2004a) as well as field-based searches for dissected terrace-like flat topographic features consistent with previously established terrace elevations. These were then field-verified by on-site analysis of soil depth, presence of cobbles, and geomorphic expression throughout the area.

Samples were prepared for chemical and mineralogical analysis according to the following methods. Bulk soils were wet sieved to remove the >2 mm material. The <2 mm fraction was split, and one sub-sample was settled in Atterburg cylinders to obtain the <2 μm fraction for analysis of clay-sized mineral content. Oriented sample mounts of the <2 μm fraction were made for XRD analysis using a Buchner Funnel membrane filtration system with 0.45 μm filters (Drever, 1973). Ethylene glycol-solvation (Hillier and Ryan, 2002) and formamide-solvation (Churchman *et al.*, 1984) methods were used to distinguish halloysite from disordered kaolinite. Samples were analyzed in the

Table 1. Information on sample sites. Site IDs represent terrace or landform sampled (e.g. AS, Qt) with relative age rank of terraces (*e.g.* Qt-3, where smaller numbers indicate older terraces), duplicate sites on a single terrace (e.g. Qt-5-1, Qt-5-2) and soil horizon and depth (B1 = 10 cm, B2 = 20 cm, B3 = 1 m, with each successive horizon indicating an additional 1 m of soil depth). Terrace ages in plain text are from Sak *et al*. (2004a) and those in bold were determined by this study. Note that all terraces formed at different paleo-sea levels. DK = disordered kaolinite; S = smectite.

Site ID	Landform, age	Elevation (masl)	Elevation above Rio Parrita (m)	Soil horizons sampled	Tectonic block	Uplift rate (m/ka)	Dominant clays
AS-1	Active river channel	~6 m	0	B1	N/A	N/A	Sm,H
AS-2	Active river channel	~20 m	0	B1	N/A	N/A	Sm,H
Qt-5-1	**Mid-Holocene terrace, ~5 ka**	~24 m	5	B1	Parrita Block	**1.0**	Sm
Qt-5-2	**Mid-Holocene terrace, ~5 ka**	~15 m	5	B1	Parrita Block	**1.0**	Sm
Qt-5-3	**Mid-Holocene terrace, ~5 ka**	24 m	5	B1, B2	Parrita Block	**1.0**	Sm
Qt-5-4	**Mid-Holocene terrace, ~5 ka**	~5 m	5	B1, B2	Esterillos Block	**1.0**	Sm
Qt-4	**Early-Holocene terrace, ~10 ka**	~20 m	10	B1,2,3,4 & C1,2,4,5,6	Esterillos Block	**1.0**	Sm, DK
Qt-3-1	**37 ka terrace**	~50 m	50	B1, B2	Esterillos Block	3.5	DK, Sm
Qt-3-2	37 ka terrace	~65 m	55	B1, B2, B3	Esterillos Block	3.5	DK, Sm
Qt-2-1	125 ka terrace	~140 m	140	B1,2,3,4,5,6,7,8			
& C1	Esterillos Block	1.2	DK				
Qt-2-2	125 ka terrace	~180 m	175*	B1, B2	Esterillos Block	1.4	DK
Qt-P-2	**125 ka terrace**	~31 m	13	B1, B2	Parrita Block	**0.1**	DK
Qt-P-1	**~Older than Qt-P-2 ⩾125 ka**	~33 m	15	B1, B2, B3	Parrita Block	**0.1**	DK

*Note: the Esterillos block is tectonically tilted to the west which accounts for the elevation difference between Qt-2-1 and Qt-2-2.

air-dried, ethylene glycol solvated (60ºC, >24 h) and heated states (250ºC). For all other mineralogical and chemical analyses, another split of the <2 mm fraction was oven dried at 60ºC. For quantitative XRD analysis, 3.6 g of dried, sieved sample were combined with 0.4 g of zinc oxide (ZnO) and 10−15 mL of distilled water and micronized in a McCrone mill for 12 min to produce a slurry of <10 μm particles. Milled powders were prepared for XRD analysis by spray drying (Hillier, 1999). Spray-dried powders were then mounted onto a zero background quartz plate and analyzed with a Siemens D-500 X-ray diffractometer operating at 40 kV and 40 mA with 0.05º2θ steps, 2 s counts, and CuKα radiation. Peak intensities for quantitative analysis were determined by measuring integrated areas using Jade® software (http://www.mdi.com) using an approach similar to that of Środoń *et al.* (2001). The XRD peaks and mineral intensity factors (MIFs; data presented are relative to the ZnO 100 peak at 2.81 Å) used in mineral quantification are presented below with detection limits (DL; based on 3 s.d. above background):

plagioclase feldspar − the 002 peak at 3.20 Å (MIF = 0.67, DL = 1%) and for verification the 201 peak at 4.04 Å (MIF = 0.22);

augite − the 22$\bar{1}$ peak at 2.99 Å (MIF = 0.31; DL = 2%);

quartz − the 101 peak at 3.34 Å (MIF = 1.71; DL = 0.4%) and the 100 peak at 4.26 Å (MIF = 0.33) for verification;

hematite − the relatively sharp 104 peak at 2.70 Å (MIF = 0.61; DL = 1%) on the low-angle side of the goethite 013 peak at 2.69 Å;

goethite − the 013 peak at 2.69 Å (MIF = 0.19; DL = 4%) with the sharp 2.70 Å peak subtracted from its area. The 4.18 Å goethite 011 peak was not used because of overlaps with the quartz 100 peak and the kaolin 02,11 peak;

magnetite − the 2.96 Å 220 peak (MIF = 0.38; DL = 2%) and the 311 peak at 2.53 Å (MIF = 1.13) for verification;

kaolin − the 001 peak at 7.2 Å (MIF = 0.20; DL = 4%);

smectite − the 001 peak at 12−15 Å (MIF = 0.45; DL = 2%);

total dioctahedral clay – to verify our results for Σ(kaolin + smectite), we measured the 060 peak at 1.49 Å (MIF = 0.09; DL = 8%). Variability was within 10% of Σ(kaolin + smectite) values obtained from 001 peaks for all samples.

ZnO peaks at 2.81 Å (100 peak), 2.60 Å (002 peak), and 2.47 Å (103 peak) were used for quantification.

Major and trace element concentrations were determined by inductively coupled plasma-atomic emission spectrometry (ICP-AES) after fusion at 1050ºC with lithium metaborate flux (Bestland *et al.*, 1997) using a Thermo-Jarrell Ash Iris 1000. Prior to fusion, samples were dried in an oven at 100ºC to drive off adsorbed water, and loss on ignition (LOI) was determined at 1050ºC. Table 2 compares our ICP analysis of Geological Survey of Canada basalt standard MRG-1 with certified values. Uncertainty determined by replicate analysis and comparison to the MRG-1 standard are $\leqslant$3% for all major elements except K_2O and MgO, for which uncertainties are $\leqslant$5%. Uncertainties for trace elements are $\leqslant$10%. Soil matrix grain-size distributions (<2 mm fraction) were measured using a Horiba LA-920 Laser Particle Size Analyzer after ultrasonic disaggregation with Calgon® deflocculating powder. Particle morphologies and compositions were examined by scanning electron microscope (SEM) analysis of carbon-coated soil aggregates fixed onto Al stubs. Four soil samples representing Qt-2-2-B2, Qt-P-1-B2, Qt-4-B2, and Qt-5-4-B2 were analyzed using an FEI Company XL-30 ESEM-FEG operating at an accelerating voltage of 15 kV; energy dispersive spectroscopy (EDS) was performed using an Edax light element Si(Li) detector. The spot size varied from 5 to 2 µm depending on the magnification.

RESULTS

Physical properties

All terraces contain rounded rock clasts (or very weathered ghost clasts in Qt-2 and Qt-P terraces) in fine-grained matrix, and the topographic expression of the terraces ranges from extensive flat plains in Qt-5 to dissected flat-topped landforms in Qt-4 and older terraces. Soils developed from weathering of terrace sediments range from poorly-developed, dark yellowish brown (10YR 3/4) Inceptisols (Qt-5) to lateritic, dark red (10R 3/6) Oxisols in the oldest terraces (Qt-2). The B horizon in 10 ka Qt-4 is 2 m deep; in 125 ka Qt-2 it is 7 m deep. Soil structure is generally angular blocky and firm in the upper B horizons. Clast size varies from fine pebbles to cobbles, and weathering rinds are progressively thicker with increasing elevation and terrace age (Sak *et al.*, 2004a).

Particle size as measured by mean, median and mode is marked by logarithmic decrease with age (Figure 2). A dramatic decrease in median particle size from 45 µm to 6 µm occurs within the first 37 ka; from 37 ka to 125 ka, the curve asymptotically approaches a slope of zero and a median particle size of 5–6 µm. Soils $\leqslant$10 ka exhibit unimodal distributions; soils $\geqslant$37 ka exhibit bimodal distributions characterized by a residual peak at 10 µm and a peak at 0.5 µm that increases in intensity with age, to the point that 10 µm and 0.5 µm peaks are equal in area in Qt-2 B horizons. Particle size values from Qt-P-2 and Qt-P-1 terraces (Parrita block) are very similar to values from the Esterillos block Qt-2 terraces.

Quantitative mineralogy of soil matrix

The results of quantitative mineral analysis are summarized in Table 3 and in Figures 2 and 3. Active sediments (AS) deposited on the 1–2 year floodplain are characterized by smectite (40–43%), kaolin (11–20%), sodic plagioclase (12–14%), augite (3–5%), goethite (6–7%), and quartz (9–12%). Sediments in the youngest, broad terrace (Qt-5) are characterized by smectite (55–73%), quartz (6–12%), plagioclase (4–9%), augite (2.2–2.3%), and kaolin (0–10%). Qt-4 B horizons are characterized by smectite (25–41%), kaolin (23–33%), quartz (10–13%), goethite (6–8%), and lesser plagio-

Table 2. Comparison of certified values from Geological Survey of Canada basalt standard MRG-1 with the results obtained as part of this study by lithium metaborate fusion and ICP-AES analysis.

Comparison of standard sample and certified values – major elements (wt.%)	Al_2O_3	CaO	Fe_2O_3	K_2O	MgO	MnO	Na_2O	SiO_2	TiO_2
Certified MRG-1 values	8.62	14.97	17.99	0.18	13.68	0.17	0.72	39.86	3.74
Midd MRG-1 values	8.54	14.68	18.55	0.19	14.41	0.10	0.71	39.05	3.78
% deviation	−0.9	−1.9	+3.1	+5.6	+5.3	−41.2	−1.4	−2	+1.1

Comparison of standard sample and certified values – trace elements (ppm)	Ba	Co	Cr	Cu	Ni	Sc	Sr	V	Y	Zn	Zr
Certified MRG-1	50	90	475	135	195	54	260	520	16	190	105
Midd MRG-1	51	86	473	143	208	56	270	536	15	197	104
% deviation	+2	−4.4	−0.4	+5.9	+6.7	+3.7	+3.8	+3.1	−6.3	+3.7	−0.9

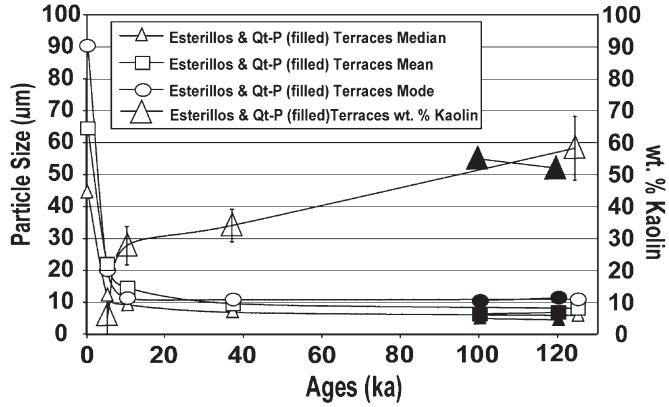

Figure 2. Median, mean and mode particle size and weight % disordered kaolinite plotted against terrace age. Values for terraces are averages of median, mean and mode for B horizon samples of that particular age terrace, yielding individual values for each terrace (Qt-5, Qt-4, Qt-3, Qt-2) and one value for parent material (AS). Qt-P-1 and Qt-P-2 ages are speculative and are plotted separately to enhance later interpretations.

clase (0–3%). Qt-4 C horizons are characterized by smectite (64–85%), plagioclase (4–16%), augite (0–3%), goethite (3–7%), and quartz (6–9%). Qt-3 and Qt-2 terrace soils contain kaolin (30–70%), FeO_x (goethite and hematite) (3–13%), and increased amounts of quartz (10–30%) relative to Qt-5 and Qt-4 (Table 3; Figure 7). The Qt-2-1 C horizon sample is dominated by kaolin (47%), FeO_x (5%), quartz (26%), and traces of smectite (<3% by QXRD; identified in <2 μm XRD patterns). Magnetite occurs throughout the sequence at concentrations of 0–2.6%. The average wt.% of kaolin increases from 0–10% in Qt-5 to 35% in Qt-3 to 59% in Qt-2 (Figure 2), an increase that follows a parabolic trend. The presence of 11–36% X-ray amorphous matter in B horizons is suggested by mineral sums that fall short of 100% (Table 3). This type of approach was applied previously in our lab by Kautz and Ryan (2003), who found that QXRD sums and oxalate extractions agree reasonably well, with QXRD indicating a mean of 21% X-ray amorphous material, and oxalate extraction

Table 3. Results of quantitative XRD analysis (QXRD). Values are in weight % of the specified minerals.

Sample ID	Quartz	Plagioclase	Pyroxene (augite)	Magnetite	Goethite	Hematite	Beidellite	Kaolin	Total
AS-1	8.9	11.8	3.6	1.5	5.9	n.d.	43.5	10.7	85.9
AS-2	12.3	13.8	4.6	1	6.4	n.d.	40.8	21.1	101.8
Qt-5-3-B2	5.9	3.7	2.2	0.5	4.4	n.d.	73.3	10.2	100.2
Qt-5-4-B2	12.3	8.9	2.3	n.d.	6.9	n.d.	55.9	n.d.	86.3
Qt-4-B1	9.7	2.3	n.d.	n.d.	8.1	n.d.	41.4	27.2	88.7
Qt-4-B2	13.3	3.2	n.d.	n.d.	6.7	n.d.	39.7	22.9	85.8
Qt-4-B3	13.2	n.d.	n.d.	n.d.	5.9	n.d.	25.1	32.8	77
Qt-4-C1	5.9	9.2	n.d.	0.6	6.4	n.d.	77.5	n.d.	99.6
Qt-4-C2	6.1	12.1	2.4	0.8	3.6	n.d.	74.8	n.d.	99.8
Qt-4-C4	7.2	10.5	2.2	1.0	4.5	n.d.	76.3	n.d.	101.7
Qt-4-C5	8.5	4.2	2.2	0.6	n.d.	n.d.	85.4	n.d.	100.9
Qt-4-C6	8.9	15.9	3.4	n.d.	n.d.	n.d.	63.9	n.d.	92.1
Qt-3-1-B2	25.2	n.d.	n.d.	2.6	1.8	4.5	n.d.	37.7	71.8
Qt-3-2-B2	29.6	n.d.	n.d.	1.0	n.d.	2.8	n.d.	30.4	63.8
Qt-2-1-B1	23.2	n.d.	n.d.	1.5	3.3	7.2	n.d.	44.2	79.4
Qt-2-1-B2	19.8	n.d.	n.d.	2.5	3.5	9.7	n.d.	49.1	84.6
Qt-2-1-B3	18.6	n.d.	n.d.	2.3	3.0	8.4	n.d.	69.7	91.3
Qt-2-1-B5	11.4	n.d.	n.d.	2.3	2.4	3.7	n.d.	59.3	79.1
Qt-2-1-B8	10.7	n.d.	n.d.	1.1	2.3	3.9	n.d.	61.5	79.5
Qt-2-1-C1	26.1	n.d.	n.d.	1.9	1.5	3.4	n.d.	47.0	79.9
Qt-2-2-B2	13.4	n.d.	n.d.	1.3	2.9	6	n.d.	68.1	91.7
Qt-P-2-B2	12.6	n.d.	n.d.	2.1	3.8	8	n.d.	55.3	81.8
Qt-P-1-B2	14.7	n.d.	n.d.	1.9	1.7	6.2	n.d.	52.4	76.9

n.d. – not detected. Note that QT-4 and QT-2-1 are 8 m deep profiles. See text for detection limits.

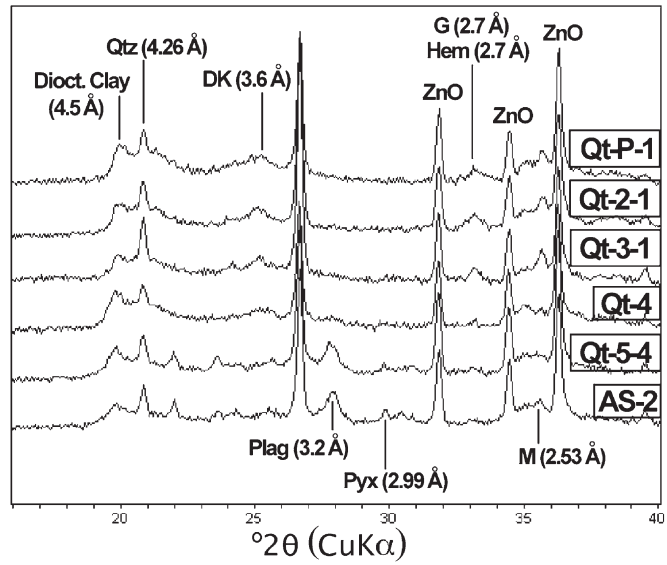

Figure 3. Representative XRD patterns used in quantitative mineral analysis. Shown are the <2 mm fraction of B2 horizons; terrace age increases from bottom to top. Progression shows the 16–40°2θ section of the pattern and highlights the plagioclase-, pyroxene- and smectite-bearing nature of younger terraces; the older, more weathered terraces are dominated by halloysite, goethite, hematite and magnetite. All samples were spray dried with 10% ZnO as an internal standard. DK = disordered kaolinite; Qtz = quartz; Plag = plagioclase; Pyx = pyroxene (augite); G = goethite; Hem = hematite; M = magnetite; Dioct. Clay = dioctahedral clay; ZnO = zinc oxide added as internal standard.

indicating a mean of 18%. Lastly, note the similarity in mineralogy of the two Parrita block terraces (Qt-P-2, Qt-P-1) and Qt-2 on the Esterillos block.

Clay mineralogy of soil matrix

The mineral content of the clay-size fraction of soil matrix ranges from smectite-dominated modern river sediment (AS-1,2) and Qt-5 terraces to disordered kaolinite-dominated Qt-3 and Qt-2 terraces (Figure 4). AS-1, AS-2 and Qt-5 show dominant 17 Å smectite 001 peaks (EG) and distinct 8.5 Å 002 peaks (EG) that occur as shoulders on kaolin 001 peaks (Figure 5). Qt-4 contains an intermediate clay mineral assemblage with an average ratio of smectite to disordered kaolinite of

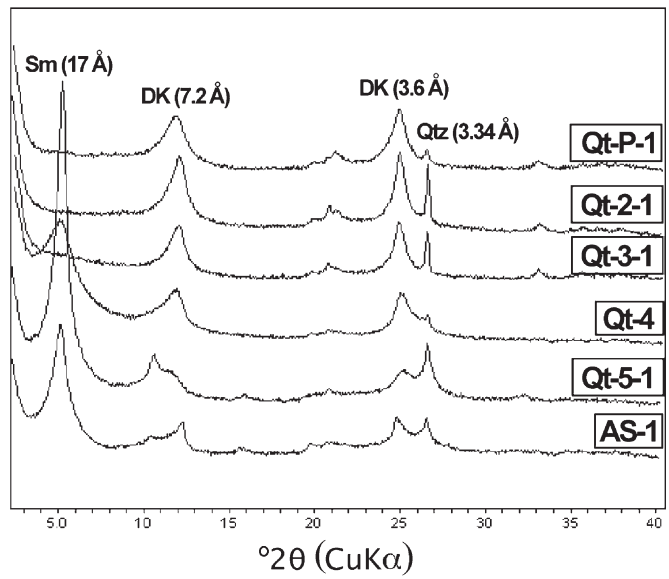

Figure 4. XRD data for ethylene glycol (EG)-solvated <2 μm oriented powders for the terrace progression; age and elevation increase from the bottom to the top (with the exception of the elevation of Qt-P-1; see text). Sm = smectite. Other symbols are as indicated in Figure 3.

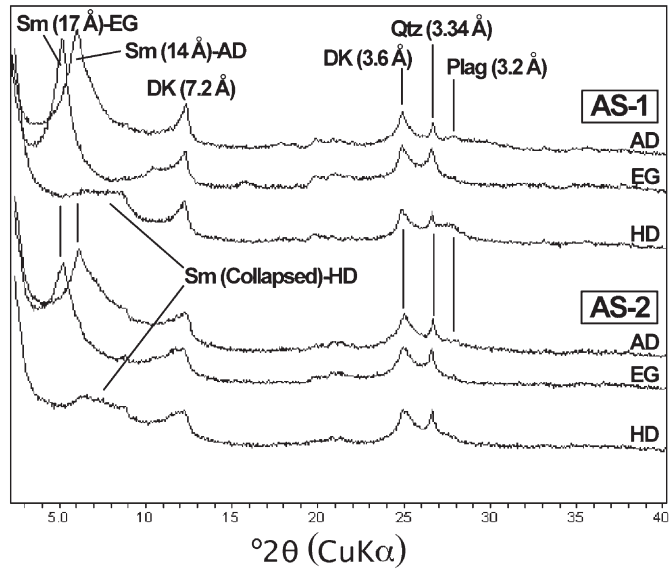

Figure 5. XRD data for the <2 μm fraction of Rio Parrita sediment (AS-1, AS-2). Note the characteristic expansion of smectite from air-dried (AD) to EG-solvated states, and collapse after heating to 250ºC for 1 h (HD).

~4:3 (Table 3). Smectite is evident from characteristic behavior of the 001 peak, which can be identified by variable air-dried spacings (12−15 Å), expansion to 16.9−17.1 Å with EG solvation, and subsequent collapse to 10−13 Å when heated (Moore and Reynolds, 1997). Incomplete collapse implies the presence of interlayer hydroxy-Al complexes (Moore and Reynolds, 1997; Ndayiragije and Delvaux, 2003). The presence of a 1.495 Å peak, and lack of trioctahedral clay peaks in random XRD mounts of smectite-rich powders, indicates that the smectite is dioctahedral (a finding confirmed by SEM-EDX – see below). Disordered kaolinite was identified by 00*l* peaks at 7.2 Å and 3.60 Å, a disordered 02*l* −11*l* band beginning at 4.48 Å, limited response to ethylene glycol solvation and almost complete lack of expansion with formamide treatment. Minor amounts of 7 Å halloysite (<10% of total kaolin) were indicated by slight increases in the kaolin 002:001 peak intensity ratio with ethylene glycol intercalation, a slight response to formamide and heating to 250ºC (1 h) that produces narrower 00*l* peaks consistent with the collapse of small amounts of hydrated layers (Churchman *et al.*, 1984).

We found no evidence for interstratified kaolin-smectite (K-S) according to XRD criteria outlined by Cradwick and Wilson (1972), Moore and Reynolds (1997) and Righi *et al.* (1999) and by comparison to NEWMOD-simulated patterns (Reynolds and Reynolds, 1997). Esterillos smectite peaks are sharp and do not exhibit broad EG *d* spacings >17.5 Å or irrational 00*l* patterns that are typical of randomly interstratified K-S. Our XRD data also lack the presence of an S(002)-K(001) peak at 7.5−7.8 Å as a low-angle shoulder on the kaolin 001 peak that expands to 7.9 Å with heating (Wilson and Cradwick (1972), further demonstrating the absence of K-S. The low-angle shoulder at 8.5 Å in Esterillos-Parrita samples is the smectite 002 peak.

The XRD patterns of air-dried, ethylene glycol-solvated, and heated powders are presented in Figure 5 to illustrate mineral identification criteria. However, EG powder patterns are displayed in the remaining figures to provide greater resolution in identifying smectite and kaolin.

Clay mineralogy of Qt-4 and Qt-2-1 soil profiles

The mineral transformations observed in the terrace progression are also evident in two deep soil exposures of the Qt-4 and Qt-2-1 terraces, where less-weathered C horizon material has observable smectite that passes upwards, either partially or fully, to disordered kaolinite in the B horizons.

In the case of Qt-4, the C horizon is dominated by smectite, while the B horizon is characterized by sub-equal amounts of smectite and disordered kaolinite (Figure 6). This transition is evident in the 002 kaolin peak, with weak kaolin peaks in the C horizon that abruptly give way to stronger kaolin peaks at the B horizon boundary. The progression from smectite-dominated to smectite- and kaolin-dominated soil is coincident with field indicators (clast weathering, matrix color) that indicate progression from less weathered C horizon material to more weathered B horizon soils.

In the Qt-2-1 profile the C horizon is marked by distinct smectite and disordered kaolinite peaks; the B horizon is dominated by disordered kaolinite peaks with very weak to non-existent smectite peaks (Figure 7). The presence of smectite in the C horizon that trends to disordered kaolinite with increased weathering provides

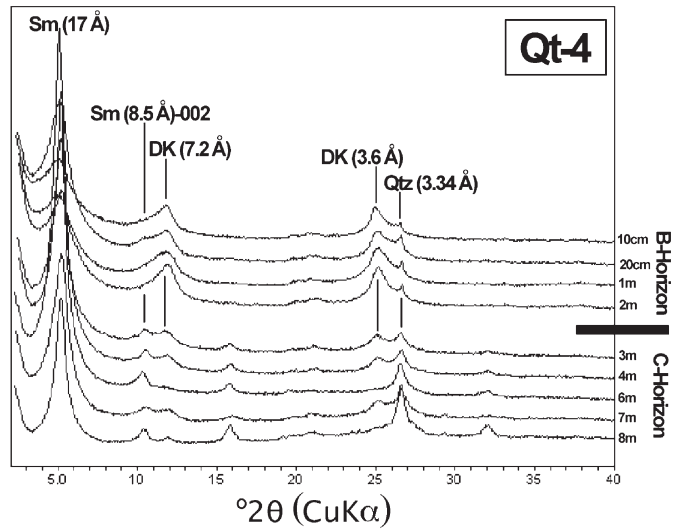

Figure 6. XRD data for the <2 μm fraction of EG-solvated powders from the 8 m Qt-4 (10 ka) terrace profile with delineated soil depths and B and C horizons.

a vertical *in situ* weathering profile that mirrors that of the terrace progression as a whole (Figure 4).

Geochemical data

Major element geochemical data for the terrace soils are presented in Table 4. Chemical weathering over 125 ka has produced expected trends for major elements (Figure 8), producing the following hierarchy of cation mobility: Ca > Na > Mg > K > Si > Al > Fe > Ti. Base cations are depleted by leaching and relatively insoluble higher-charge cations like Fe, Al, Zr and Ti are residually concentrated. The curve depicting base cation depletion shows marked decrease from Qt-5 to Qt-3 but little variation from Qt-3 to Qt-2, where the sum of base cations (expressed as ΣNa_2O, MgO, K_2O, CaO) levels off at 1.0 wt.%. Fe displays parabolic enrichment that mirrors depletion of base cations – rapid enrichment occurs from Qt-5 (9% Fe_2O_3) to Qt-3 (17% Fe_2O_3) and little difference exists between Qt-3 and Qt-2 terraces (17–20% Fe_2O_3). Enrichment of Zr (136 ppm in AS to 247 ppm in Qt-2) suggests mass losses of nearly 50% by weight in Qt-2 soils and Sr displays a similar depletion trend to the base cations (280 ppm in AS to 19 ppm in Qt-2; Figure 9). Qt-P terraces are geochemically similar to Qt-2 terraces with a few exceptions such as wt.% Fe_2O_3 and TiO_2, both of which show slightly higher values for Qt-P terraces than Qt-2 terraces (Table 4; Figure 8), and pH.

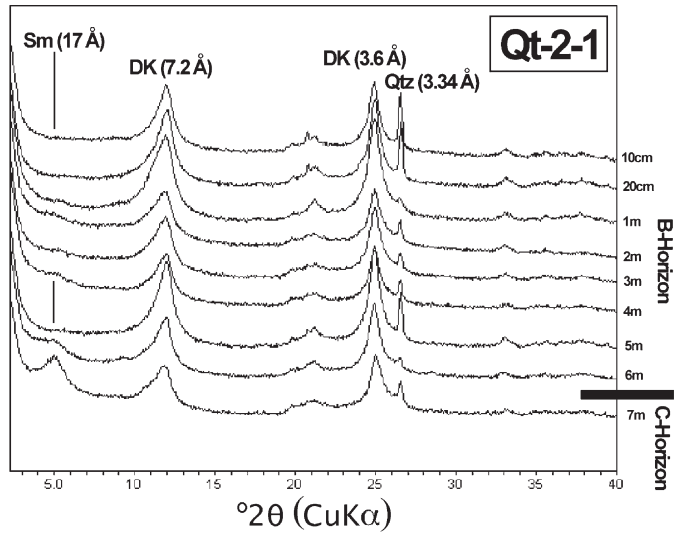

Figure 7. XRD data for the <2 μm fraction of EG-solvated powders from the 7 m Qt-2-1 terrace (125 ka) profile with delineated soil depths and B and C horizons.

Table 4. Major element geochemistry (wt.%) determined by ICP-AES on bulk (<2 mm) soil matrix.

Sample ID	Al_2O_3	CaO	Fe_2O_3	K_2O	MgO	MnO	Na_2O	SiO_2	TiO_2	LOI	Sr	Zr
AS-1	20.87	3.20	12.08	1.09	3.58	0.11	1.33	56.34	1.40	10.8	281	133
AS-2	18.74	3.42	12.29	1.17	4.22	0.10	1.48	57.03	1.55	8.4	280	140
Qt-5-3-B1	17.93	1.76	18.22	0.74	6.56	0.23	0.36	51.45	2.74	13.0	134	195
Qt-5-3-B2	17.05	2.05	17.47	0.72	8.52	0.16	0.25	51.06	2.71	12.5	144	184
Qt-5-4-B1	16.38	3.20	13.16	1.30	2.25	0.03	1.53	60.11	2.05	8.5	288	157
Qt-5-4-B2	17.97	2.41	13.04	1.43	2.52	0.03	1.29	59.38	1.93	8.5	238	164
Qt-4-B1	23.66	0.27	18.53	0.39	1.62	0.04	0.31	52.40	2.78	13.2	58.0	199
Qt-4-B2	21.61	0.24	18.19	0.46	1.61	0.01	0.35	55.76	1.78	12.0	62.8	191
Qt-4-B3	27.47	0.11	10.62	0.56	1.61	0.00	0.10	57.30	2.24	12.2	35.8	200
Qt-4-B4	23.21	0.48	16.24	0.58	1.83	0.06	0.48	54.78	2.34	11.7	92.4	187
Qt-4-C1	17.34	1.75	20.09	0.75	3.00	0.08	1.37	53.12	2.50	9.4	185	156
Qt-4-C2	18.70	2.37	13.40	0.67	3.54	0.08	1.49	57.35	2.41	9.2	196	157
Qt-4-C4	15.40	3.22	15.00	1.12	3.78	0.05	1.77	57.51	2.14	8.8	227	147
Qt-4-C5	18.38	2.03	12.69	0.80	3.48	0.03	1.17	59.58	1.84	10.0	141	149
Qt-4-C6	17.06	3.44	10.94	1.28	3.40	0.04	2.18	59.86	1.79	8.0	217	135
Qt-3-1-B1	16.38	0.19	18.87	0.22	0.39	1.38	0.04	58.98	3.54	11.1	39.6	266
Qt-3-1-B2	17.42	0.13	19.45	0.28	0.53	1.47	0.07	57.20	3.47	10.4	31.3	255
Qt-3-2-B1	16.14	0.26	15.26	0.41	0.52	0.12	0.09	64.87	2.33	10.7	48.1	254
Qt-3-2-B2	18.24	0.17	15.62	0.36	0.69	0.09	0.05	62.48	2.28	10.5	45.9	244
Qt-3-2-B3	29.57	0.26	19.28	0.52	0.89	0.01	0.06	46.74	2.67	13.3	48.4	271
Qt-2-1-B1	19.29	0.11	17.44	0.27	0.47	0.25	0.08	59.53	2.57	12.5	30.1	216
Qt-2-1-B2	23.13	0.12	18.38	0.36	0.64	0.06	0.06	54.62	2.64	11.7	30.2	223
Qt-2-1-B3	24.90	0.03	20.36	0.40	0.54	0.01	0.04	50.68	3.05	11.2	12.1	259
Qt-2-1-B5	26.76	0.06	20.57	0.34	0.89	0.03	0.01	48.04	3.30	12.1	13.0	248
Qt-2-1-B7	25.17	0.16	19.19	0.48	0.50	0.04	0.19	51.44	2.83	11.7	14.4	276
Qt-2-1-B8	26.36	0.04	21.61	0.35	1.10	0.11	0.03	47.40	3.00	12.0	10.9	230
Qt-2-1-C1	21.05	0.04	17.90	0.59	1.09	0.09	0.04	57.00	2.20	9.5	14.5	204
Qt-2-2-B1	25.87	0.11	19.53	0.39	0.34	0.17	0.16	50.72	2.70	12.2	24.3	274
Qt-2-2-B2	27.39	0.03	20.14	0.32	0.42	0.11	0.04	48.84	2.70	12.7	19.8	254
Qt-P-2-B1	26.81	0.26	23.04	0.37	0.64	0.09	0.15	45.29	3.35	13.6	33.7	252
Qt-P-2-B2	27.72	0.09	23.02	0.37	0.59	0.07	0.01	44.65	3.48	12.2	23.8	271
Qt-P-1-B1	27.43	0.24	22.32	0.80	0.60	0.02	0.49	44.95	3.15	12.8	26.7	257
Qt-P-1-B2	26.54	0.04	20.81	0.35	0.59	0.01	0.05	48.63	2.97	11.7	20.9	270

Values were normalized to 100% on an anhydrous basis (raw un-normalized sums ranged from 95 to 100%). Sr and Zr are in mg/kg (ppm).

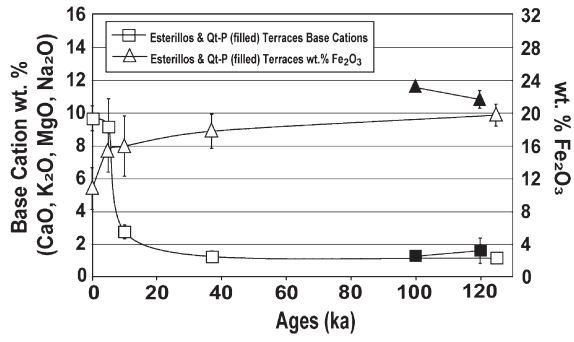

Figure 8. Base cation wt.% (ΣNa_2O, MgO, K_2O, CaO) and wt.% Fe_2O_3 from ICP-AES analyses plotted against terrace age. The values are the averages of individual B horizon samples of that particular aged terrace, yielding one value for each terrace age (Qt-5, Qt-4, Qt-3, Qt-2) and parent material (AS). Qt-P ages are speculative and are plotted separately.

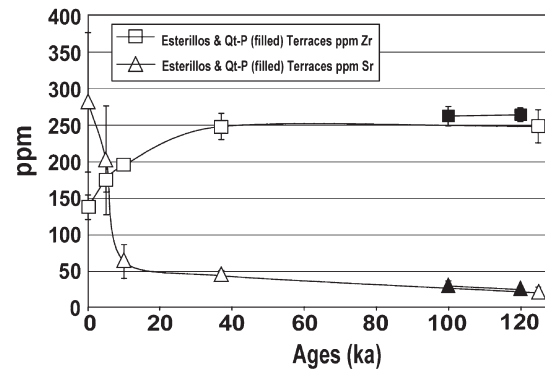

Figure 9. Concentrations of Sr and Zr (ppm) plotted against terrace age. Values for terraces are the averages of individual B horizon samples of that particular aged terrace, yielding one value for each terrace age (Qt-5, Qt-4, Qt-3, Qt-2) and parent material (AS). Qt-P ages are speculative and are plotted separately.

Soil pH (1:2 soil:water) of B horizons (<1 m depth) are as follows:

4.4–4.7 in Qt-2 and Qt-3 terraces;
5.4–5.6 in Qt-4 terraces;
6.1–6.5 in Qt-5 terraces;
7.7–7.9 in fluvial deposits on the 1-2 year floodplain (AS);
4.8–5.9 in Qt-P terraces.

Soil from the C horizon at the base of the 8 m deep Qt-4 profile has a pH of 7.4. C horizon soil from 7 m depth at Qt-2-1 has a pH value of 4.9.

SEM-EDX

Smectites from the Holocene Qt-5 (Figure 10a) and Qt-4 (Figure 10b) terraces line pore space and exhibit flaky particle morphology typical of pedogenic smectite. The EDX scans of smectite-rich pore space indicate the presence of ferruginous beidellite with a composition of $(Mg_{0.2},Ca_{0.1})(Fe_{0.6}Al_{1.4})(Si_{3.6}Al_{0.4})O_{10}(OH)_2$. This finding is consistent with XRD data indicating that the smectite is dioctahedral and is compositionally similar to previous analyses of ferruginous beidellite in soils (Özkan and Ross, 1979; Righi *et al.*, 1998), including the extent of tetrahedral Al substitution – note that this formula contains a +0.2 charge per formula unit imbalance, probably attributable to minor impurities within the areas scanned by EDX. Disordered kaolinite in Qt-3, Qt-2 and Qt-P terraces occurs as spheroidal particles of ~0.1–0.5 μm in diameter (Figure 10c). Disordered kaolinite crystals in Qt-4 appear to have crystallized on beidellite surfaces.

DISCUSSION

With increasing age, soils formed on the Rio Parrita terraces exhibit distinct changes in mineral assemblage, chemical composition and texture. These changes include: (1) rapid dissolution of plagioclase, from 4–15% in parent material to undetectable in ⩾37 ka soils, and augite, from 2–5% in parent material to undetectable in ⩾37 ka soils; (2) formation of ferruginous beidellite in <15 ka soils and its complete transition to disordered kaolinite in B horizons of ⩾37 ka soils; (3) rapid loss of base cations that produces steady-state-like conditions with respect to base cation concentrations in ⩾37 ka soils; (4) reduction in grain size to a median steady state value of 5–6 μm; and (5) residual concentration of disordered kaolinite, goethite, hematite and insoluble cations (Zr, Ti, Fe, Al) that shows notably diminished rates of increase with age, suggesting a progression toward steady-state conditions for these parameters. These trends are also present vertically in 7 to 8 m deep soil profiles and are consistent with previous work on lateritic soils that show progression toward an assemblage dominated by kaolin, hematite, and goethite with increased age (Nieuwenhuyse and van Breeman, 1997).

The transition from beidellite to disordered kaolinite

Kaolin commonly forms in tropical soils in response to rapid weathering of primary minerals and similarly rapid leaching of base cations and Si (Hughes, 1980; Nieuwenhuyse and van Breeman, 1997). Disordered kaolinite is believed to form as a metastable precursor to kaolinite (Hughes, 1980) that is kinetically favored by rapid crystallization following parent rock dissolution. Either way, disordered kaolinite formation is favored by the Al- and Si-rich, base-poor soil water that characterizes most tropical soils. By comparison, the occurrence of beidellite in humid tropical soils is far less common and appears to be constrained to soils derived from weathering of basic igneous rocks (Craig and Loughnan, 1964; Kantor and Schwertman, 1974) and volcanic ash (Ndayiragije and Delvaux, 2003). Outside of the humid tropics, beidellite commonly forms in soils under Mediterranean (xeric) climates with MAP of 800–1000 mm (Özkan and Ross, 1979) and temperate climates with MAP of 1000–1500 mm (Righi *et al.*, 1998). Muhs (2001) documented smectite in <220 ka Pleistocene soils formed under the subtropical climate of Barbados (MAP = 1100 mm) but did not report on the composition. The occurrence of beidellite (or any smectite) in humid tropical soils clearly reflects ephemeral conditions characterized by relatively high

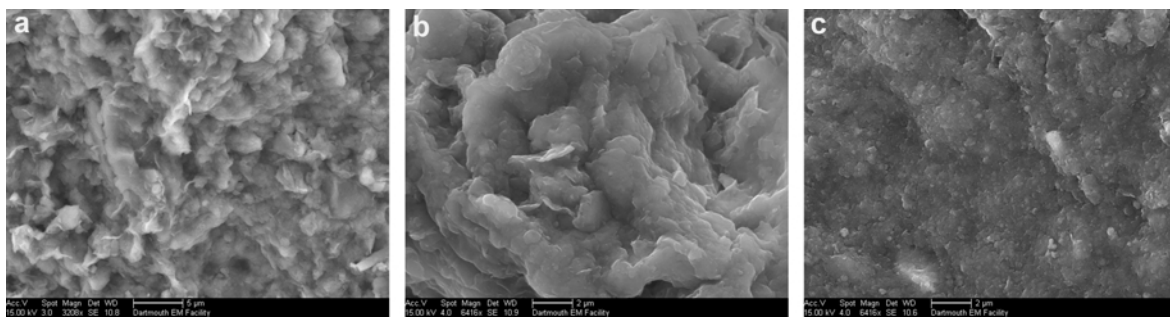

Figure 10. SEM images of soil matrices showing: (a) the flaky particle morphology of smectite in the Qt-5-1-B2 soil matrix; (b) the flaky smectite and spheroidal disordered kaolinite in the Qt-4-B2 soil matrix; and (c) the abundant spheroidal disordered kaolinite in the Qt-2-2-B2 bulk soil aggregate. Scale bars for a = 5 μm; for b, c = 2 μm.

pH (>5) and high concentrations of dissolved base cations, Fe, Al and Si in soil water, conditions produced by rapid primary mineral decomposition in young soils not yet leached to the Al-Fe-Si-dominated composition typically associated with humid tropical climates. Whereas beidellite appears to persist over time periods approaching 10^6 years in drier climates where evapotranspiration exceeds leaching (Özkan and Ross, 1979), beidellite in leaching-dominated soils where precipitation far exceeds evapotranspiration can only be considered a metastable precursor to kaolin. Also, Herbillon *et al.* (1981), Yerima *et al.* (1985) and Righi *et al.* (1999) illustrate the importance of drainage, where smectite predominates in poorly drained footslope sections of toposequences, kaolin in well-drained sections, and K-S in between in soils of moderate drainage.

While the transition of soil smectite to kaolin with prolonged weathering has been observed elsewhere (Altschuler *et al.*, 1963; Herbillon *et al.*, 1981; Yerima *et al.*, 1985; Muhs, 2001), to the best of our knowledge only Muhs (2001) has constrained the kinetic nature of the transition in soil environments. In the relatively dry subtropics of Barbados, smectite persists in soils up to 220 ka, where it is replaced by interstratified K-S in soils 220−460 ka, and ultimately, kaolin in 700 ka soils. In the humid tropics of Esterillos, Costa Rica, beidellite is completely altered to disordered kaolinite within 37 ka.

Numerous studies document transitions from smectite to kaolin that take place *via* intermediate K-S, a reaction pathway that is fostered by loss of Si and base cations with increasing intensity and duration of weathering (*i.e.* S → K-S → K) (*e.g.* Herbillon *et al.*, 1981; Yerima *et al.*, 1985; Righi *et al.*, 1999). However, in the Esterillos region the transition of smectite to disordered kaolinite occurs with no intermediate K-S; likewise, no K-S was found in the humid tropical soils of La Selva in eastern Costa Rica where MAP = 4000 mm (Nieuwenhuyse and van Breeman, 1997; Kautz and Ryan, 2003). This precipitation value stands in contrast to K-S bearing soils (Yerima *et al.*, 1985) in El Salvador, where MAP = 1800 mm, and elsewhere, where K-S occurs in soils where MAP = 500−2000 mm (*e.g.* Burundi, western Cameroon, northern Italy − Herbillon *et al.*, 1981; Delvaux *et al.*, 1990; Righi *et al.*, 1999, respectively). Given the similarity in parent materials, soil age and vegetation between Costa Rica and El Salvador, the presence of K-S in El Salvador is attributed to lower precipitation and less intense leaching that in turn preserves higher base cation concentrations and Si:Al ratios; conversely, the absence of K-S in the S → K transition in Costa Rica is attributed to rapid decrease in base cations and Si:Al ratio caused by intense leaching. Based on existing data, it appears that K-S forms as an intermediary in the S → K transition in soils where MAP is 500−2000 mm, but that S transforms to K with no intermediate K-S in soils that receive >3000 mm MAP. In the absence of K-S, the transition from beidellite to disordered kaolinite must occur via a dissolution-precipitation mechanism, where disordered kaolinite (and goethite or hematite) crystallizes via neoformation from ions released by beidellite dissolution.

The absence of 10 Å halloysite at Esterillos is attributed to irreversible dehydration to 7 Å kaolin during the dry season (Takahashi *et al.*, 1993), a situation that differs from soils to the north at La Selva, where the 10 Å form persists for 10^5 years due to lack of a dry season (Kautz and Ryan, 2003).

Weathering trends and implications for steady state

Age plots for grain size (Figure 2), base cations (Figure 8, Table 4) and Zr (Figure 9) follow parabolic trends characterized by rapid re-equilibration from floodplains to 37 ka terrace soils and steady-state conditions in 37 to 125 ka terrace soils. Other measures of soil maturity display trends that appear to be approaching, but have not yet been reached, steady-state conditions, including Fe (Figure 8) and other largely immobile elements (Table 4), as well as hematite (Table 3) and disordered kaolinite (Figure 2). Soil evolution clearly slows with time in a trajectory towards steady state, and logarithmic chronofunctions yield the highest correlation coefficients for geochemical, textural and mineralogical trends. The initial coarse-grained nature of the fluvial deposits promotes rapid infiltration and chemical weathering of primary plagioclase and augite and formation of metastable beidellite; progressive leaching of base cations and Si causes dissolution of beidellite and neoformation of disordered kaolinite, and enhances precipitation of hematite, amorphous aluminosilicates, and Fe- and Al-hydroxides. Because the $\geqslant$37 ka soils are already chemically depleted, it is likely that the fine-grained soil matrix of the older terraces creates a physical barrier to continued leaching of residual mobile elements that further enhances steady state.

If pedogenesis is viewed as the sum of progressive (*e.g.* leaching) and regressive processes (*e.g.* input of dust, physical erosion), then steady state is defined as the stage in soil development where progressive and regressive processes are equal (Johnson *et al.*, 1990). At Esterillos, progressive pedogenesis includes obvious processes such as dissolution of primary minerals, leaching of soluble ions, sequential formation of beidellite and disordered kaolinite, and residual concentration of immobile ions. Deposition of aerosols in the form of volcanic ash and dust is the main process contributing to regressive pedogenesis on relatively flat-topped landforms where physical erosion is minimal. We know of no existing data on influx of ash to these soils, and there is no obvious evidence of an ash component, but we cannot rule out periodic ash input. The study area receives Saharan aerosols from prevailing easterly winds that deposit approximately 0.5−1 kg/m^2 of dust annually

(extrapolated from data in Prospero *et al.*, 1996). Although we were unable to find data for Central America, dust deposited in Barbados contains 60% mica, 10% quartz, 6% kaolin, 6% plagioclase, 4% chlorite, 5% calcite, 3% each of microcline and gypsum, and 2% goethite (Prospero *et al.*, 1981). Saharan dust is relatively uniform in composition across the north Atlantic–Caribbean region as indicated by the similarity in dust deposited at Barbados and French Guiana (Goudie and Middleton, 2001), implying that these values are reasonable to use for Esterillos. At 0.5–1 kg/m^2/y, Esterillos soils receive 5–10 g of MgO, 25–50 g of K_2O, 20–40 g of CaO and 2–5 g of Na_2O per m^2/y from Saharan dust. At steady state, this influx rate should equal efflux by leaching. If so, Esterillos soils $\geqslant$37 ka experience leaching losses of 50–100 g of base cations (ΣMgO, K_2O, CaO, Na_2O listed above) per m^2/y plus whatever additional losses that would be required to balance ash input. No data are available on leaching losses in the study area, but for comparison, White *et al.* (1998) document leaching losses (Σwt.% oxides of base cations) of 30 g/m^2/y in highly leached kaolinitic Ultisols of the Rio Icacos watershed of humid tropical Puerto Rico. The discrepancy between the Esterillos and Rio Icacos regions may be ascribed to quartz diorite parent materials at Rio Icacos that are more siliceous and base poor than parent materials at Esterillos, assuming that ash contributions are negligible in the Esterillos region.

The rapid initial leaching of base cations observed at Esterillos also occurs at La Selva, coincident with the enrichment trends in immobile cations such as Fe, Al and Ti witnessed in the Esterillos terrace progression. The age-related trends of increasing halloysite, quartz and plagioclase are similar to those at Esterillos. The main differences between Esterillos and La Selva are (1) higher leaching rate at La Selva, and (2) lack of smectite in soils >0.1 ka at La Selva (as compared to its persistence in 10 ka Esterillos soils). At La Selva, base cations (sum of wt.% CaO, K_2O, MgO, Na_2O) reach a depleted steady-state concentration of 0.6% within 10 ka, whereas at Esterillos, base cations reach a depleted steady-state concentration of 1% after 37 ka. The differences are probably due to differences in mean annual precipitation (4015 mm at La Selva as opposed to 3085 mm at Esterillos), where lower MAP and a pronounced dry season at Esterillos would contribute to higher steady-state concentrations of base cations.

The concept of steady state in soils is not commonly discussed in soil science literature, but has been observed, particularly by Vidic and Lobnik (1997) in their study of fluvial terraces in the humid temperate climate of Slovenia. In this suite of soils, they found no significant difference in pedogenic indices of soils between the ages of 980 ka and 1800 ka, and as at Esterillos, pedogenic trends are best described by logarithmic or semi-logarithmic functions. Nordt *et al.* (2004) observed steady-state conditions in Pleistocene Vertisols in southeast Texas, and Battacharyya *et al.* (1999) documented steady-state conditions in Alfisols in the Bhimashankar plateau of NW India. Data from elsewhere also seem to indicate steady-state conditions, *e.g.* in soils from the humid tropics of Rio Icacos, Puerto Rico (White *et al.*, 1998) with respect to base cations and kaolinite, and soils from the temperate Mediterranean climate of northern California, where Merritts *et al.* (1992) show curves that imply steady state with respect to Fe and Al. Whether or not one agrees that the Esterillos soils have truly reached steady-state conditions, from a practical point of view the effective steady-state conditions with respect to base cations in post-37 ka soils in this region have important ramifications with respect to modeling soil nutrients in that $\geqslant$37 ka soils in this region are nutrient depleted and Al-rich, and thus poorly suited for agriculture and forestry without significant amendments.

The diffusion-limited nature of weathering reactions in soil matrix is clearly illustrated by the logarithmic weathering functions found in this study. This is intuitively correct given that reactions are largely driven by diffusion of mobile ions out of the soil *via* leaching losses. Interestingly, Sak *et al.* (2004a) found that the rate of weathering rind growth on basalt clasts in the same series of soils studied herein is best characterized by linear chronofunctions and modeled as interface limited. This too is intuitively correct given that rind growth is controlled by reactions at the interface of clast and soil matrix.

Implications for landscape evolution

Ages of the Qt-5 (5 ka) and Qt-4 (10 ka) terraces were constrained using geochemical, clay mineralogical, particle size parameters, and best fit to predicted power function weathering curves (Birkeland, 1999). Soils from these terraces display beidellite-dominated, base cation-rich assemblages (Table 1) consistent with their lower elevations relative to the other terraces in the Esterillos Block progression. This study provides the first age constraints for these two terraces, providing further precision for examining pedogenic and tectonic uplift rates. It is the rapid change in soil properties in pre-37 ka soils that facilitates differentiation of terraces in the Qt-5 (5 ka) to Qt-3 (37 ka) age range.

In the case of the older soils, differences are far more subtle – base cations have been leached to trace concentrations and soil clays are dominantly disordered kaolinite. However, differentiation of even the oldest terraces (37 and 125 ka) is made possible by non-steady-state conditions with respect to disordered kaolinite and Sr.

Geochemistry, clay mineralogy, and particle size data consistently show that the Qt-P-2 and Qt-P-1 Parrita block terraces correlate most closely to the 125 ka Qt-2 Esterillos terraces, and are very different from 5–10 ka terraces at similarly low elevations ($\leqslant$15 m above Rio

Parrita level) on the Esterillos Block, thus implying ages $\geqslant$125 ka for the Qt-P terraces despite their low elevations. The Qt-P terraces are located further east than all other terraces analyzed and lie east of the fault that separates the Esterillos and Parrita blocks (detailed map accessible at http://community.middlebury.edu/~pryan). The Qt-P terraces are situated in the topographically flatter, lower elevation valley ~100 m east of the higher-elevation dissected terraces, a topographical boundary that represents the geomorphic expression of the block-bounding fault, with the Esterillos Block to the NW and the Parrita Block to the SE. This finding is important because it demonstrates the applicability of this method to determining terrace ages on blocks lacking published ages. These ages can then be used in conjunction with terrace elevation to infer the block margin locations and uplift rates.

Terrace ages indicate an average uplift rate of 1 m/ka averaged over the last 125 ka on the Esterillos block, but an anomalously high uplift rate of 3.5 m/ka within the last 37 ka (Sak *et al.*, 2004a). Determination of Qt-4 and Qt-5 terrace ages in this study augment the work of Sak *et al.* (2004a, 2004b) and document an uplift rate of 4.4 m/ka from 37 to 10 ka. This increase in the uplift rate can be attributed to the subduction of an anomalous bathymetric feature at the Middle America Trench (Gardner *et al.*, 1992; Sak *et al.*, 2004b) that is believed to cause anomalous flexure within the fore-arc blocks causing differential uplift rates within a fairly short geologic period, and potentially temporary subsidence as the peak moves past the fore-arc and down the back side of the seamount (Sak *et al.*, 2004b). Given that average uplift rates for the last 125 ka are ~1 m/ka, this indicates that the average uplift rates for the period 125 to 37 ka were negligible. This finding is further supported by the lack of terraces formed during that period, in spite of high sea level stands at 100 ka and 80 ka.

In addition to differential uplift rates over time on the Esterillos Block, this study also documents a much lower uplift rate on the western margin of the Parrita Block where Qt-P-2 and Qt-P-1 are located (Table 1). If Qt-P-2 and Qt-P-1 are ~125 ka, Parrita block uplift rates are 0.1 m/ka, reflecting drastically different uplift rates of individual fault blocks over short distances (*e.g.* 5–10 km). Smaller uplift rates of the Parrita block are consistent with lower elevation and flatter topography; this finding is also consistent with other tectonic studies performed on the uplift rates of these fore-arc blocks (Fisher *et al.*, 1998), which estimate the western margin of the Parrita block as having an average uplift rate of 0.15 m/ka over the last 125 ka.

Terrace soils and Quaternary climate

Studies of Costa Rican paleoclimate based on paleoecological reconstructions indicate relative stability throughout the Quaternary (Sak *et al.*, 2004a), a finding that is confirmed by the work of White *et al.* (1998) in Puerto Rico. However, recent studies have shown that, even within the short period of the Holocene, sea-surface temperatures in both the Pacific and Atlantic have fluctuated, potentially shifting weather patterns and ocean circulation (deMenocal *et al.*, 2000). Other studies have documented large and abrupt shifts in the hydrologic cycle of the tropical Atlantic dating back as far as 90 ka (Peterson *et al.*, 2000). Lachniet and Seltzer (2002) provided evidence for periods of glaciation in the high peaks of Costa Rica in the past 140 ka. The most pronounced decreases in mean annual temperatures appear to have been confined to the highest elevations and are believed to be coincident with drier climate caused by an equator-ward restriction of the Intertropical Convergence Zone (ITCZ). MAT at ~3000 m in Chirripo National Park is currently 8ºC as opposed to 27ºC in the Esterillos region (Lachniet and Seltzer, 2002; Sak *et al.*, 2004a). When glaciers were present in the high elevations of Chirripo National Park, it is likely that the coastal region was still experiencing very mild humid tropical conditions where leaching processes would have dominated pedogenesis. Thus, while it is possible that the study area has undergone climatic fluctuations within the last 125 ka, it is unlikely that any of these changes were significant enough to greatly affect pedogenesis.

CONCLUSIONS

(1) Smectite (ferruginous beidellite) transforms to disordered kaolinite with no evidence of intermediate kaolinite-smectite.

(2) Parabolic weathering functions provide best-fit curves for weathering trends, and indicate steady-state conditions with respect to soil particle size and concentrations of base cations and Zr.

(3) Soil mineralogy, geochemistry and texture are useful in deciphering terrace age relationships and determining tectonic uplift rates. In particular, these parameters were applied to identification of previously unrecognized Holocene and Pleistocene terraces, and to constraining uplift rates, which range from values as high as 4.4 m/ka on the Esterillos Block to as low as 0.1 m/ka on the adjacent Parrita Block.

ACKNOWLEDGMENTS

This study was supported by a grant from the National Science Foundation – RUI program (EAR-0126018) and the Middlebury College Undergraduate Research Fund. We thank Georg Grathoff and an anonymous reviewer for constructive reviews that improved the manuscript, and C. Daghlian and J. Aronson for access to the Dartmouth College electron microscope facility.

REFERENCES

Altschuler, Z.S., Dwornik, E.J., and Kramer, H. (1963) Transformation of montmorillonite to kaolinite during weathering. *Science*, **141**, 148–152.

Battacharyya, T., Pal, D.K. and Srivastava, P. (1999) Role of zeolites in persistence of high altitude ferruginous Alfisols of the humid tropical Western Ghats, India. *Geoderma*, **90**, 263–276.

Bestland, E.A., Retallack, G.J. and Swisher, C.C. (1997) Stepwise climate change recorded in Eocene-Oligocene paleosol sequences from Central Oregon. *Journal of Geology*, **105**, 153–172.

Birkeland, P.W. (1999) *Soils and Geomorphology (Third Edition)*. Oxford University Press, New York.

Churchman, G.J., Whitton, J.S., Claridge, G.G.C. and Theng, B.K.G. (1984) Intercalation method using formamide for differentiating halloysite from kaolinite. *Clays and Clay Minerals*, **32**, 241–248.

Cradwick, P.D. and Wilson, M.J. (1972) Calculated X-ray diffraction profiles for interstratified kaolinite-montmorillonite. *Clay Minerals*, **9**, 395–405.

Craig, D.C. and Loughnan, F.C. (1964) Chemical and mineralogical transformations accompanying weathering of basic rocks from New South Wales. *Australian Journal of Soil Research*, **2**, 218–234.

Delvaux, B., Herbillon, A.J., Vielvoye, L. and Mestdagh, M.M. (1990) Surface properties of clay mineralogy of hydrated halloysitic soil clays. II: evidence for the presence of halloysite/smectite (H/Sm) mixed-layer clays. *Clay Minerals*, **25**, 141–160.

deMenocal, P., Ortiz, J., Guilderson, T. and Sarnthein, M. (2000) Coherent high- and low-latitude climate variability during the Holocene warm period. *Science*, **288**, 2198–2202.

Drever, J.I. (1973) The preparation of oriented clay mineral specimens for X-ray diffraction analysis by a filter membrane peel technique. *American Mineralogist*, **58**, 553–554.

Fisher, D.M., Gardner, T.W., Marshall, J.S., Sak, P.B. and Protti, M. (1998) Effect of subducting sea-floor roughness on fore-arc kinematics, Pacific coast, Costa Rica. *Geology*, **26**, 467–470.

Gardner, T.W., Verdonck, D., Pinter, N.M., Slingerland, R., Furlong, K.P., Bullard, T.F. and Wells, S.G. (1992) Quaternary uplift astride the aseismic Cocos Ridge, Pacific coast, Costa Rica. *Geological Society of America Bulletin*, **104**, 219–232.

Goudie, A.S. and Middleton, N.J. (2001) Saharan dust storms: nature and consequences. *Earth-Science Reviews*, **56**, 179–204.

Harris, S.A., Neumann, A.M. and Stouse, A.D. Jr (1971) The major soil zones of Costa Rica. *Soil Science*, **112**, 439–451.

Herbillon, A.J., Frankart, R. and Vielvoye, L. (1981) An occurrence of interstratified kaolinite-smectite minerals in a red-black soil toposequence. *Clay Minerals*, **16**, 195–201.

Hillier, S. (1999) Use of an air brush to spray dry samples for X-ray powder diffraction. *Clay Minerals*, **34**, 127–135.

Hillier, S. and Ryan, P.C. (2002) Identification of halloysite (7Å) by ethylene glycol solvation: the 'MacEwan effect'. *Clay Minerals*, **37**, 487–496.

Hughes, J.C. (1980) Crystallinity of kaolin minerals and their weathering sequence in some soils from Nigeria, Brazil and Colombia. *Geoderma*, **24**, 317–325.

Johnson, D.L., Keller, E.A. and Rockwell, T.K. (1990) Dynamic pedogenesis: new views on some key soil concepts and a model for interpreting soils. *Quaternary Research*, **33**, 306–319.

Kantor, W. and Schwertmann, U. (1974) Mineralogy and genesis of clays in red-black soil toposequences on basic igneous rocks in Kenya. *Journal of Soil Science*, **25**, 67–78.

Kautz, C.Q. and Ryan, P.C. (2003) The 10 Å to 7 Å halloysite transition in a tropical soil sequence, Costa Rica. *Clays and Clay Minerals*, **51**, 252–263.

Lachniet, M.S. and Seltzer, G.O. (2002) Late Quaternary glaciation of Costa Rica. *Geological Society of America Bulletin*, **114**, 547–558.

Merritts, D.J., Chadwick, O.A., Hendricks, D.M., Brimhall, G.H. and Lewis, C.J. (1992) The mass balance of soil evolution on late Quaternary marine terraces, northern California. *Geological Society of America Bulletin*, **104**, 1456–1470.

Meybeck, M. (1987) Global chemical weathering of surficial rocks estimated from dissolved river loads. *American Journal of Science*, **287**, 401–428.

Moore, D.M. and Reynolds, R.C. Jr. (1997) *X-ray Diffraction and the Identification and Analysis of Clay Minerals*. Oxford University Press, New York, 378 pp.

Muhs, D.R. (2001) Evolution of soils on quaternary reef terraces of Barbados, West Indies. *Quaternary Research*, **56**, 66–78.

Ndayiragije, S. and Delvaux, B. (2003) Coexistence of allophane, gibbsite, kaolinite and hydroxy-Al-interlayered 2:1 clay minerals in a perudic Andosol. *Geoderma*, **117**, 203–214.

Nieuwnhuyse, A. and van Breemen, N. (1997) Quantitative aspects of weathering and neoformation in selected Costa Rican volcanic soils. *Soil Science Society of America Journal*, **61**, 1450–1458.

Nordt, L.C., Wilding, L.P., Lynn, W.C. and Crawford, C.C. (2004) Vertisol genesis in a humid climate of the coastal plain of Texas, U.S.A. *Geoderma*, **122**, 83–102.

Özkan, A.I. and Ross, G.F. (1979) Ferruginous beidellites in Turkish soils. *Soil Science Society of America Journal*, **43**, 1242–1248.

Pazzaglia, F.J., Gardner, T.W. and Merritts, D. (1998) River longitudinal profiles and bedrock incision models: stream power and the influence of sediment supply. Pp. 207–236 in: *Rivers over Rock: Fluvial Processes in Bedrock Channels* (E. Wohl and K. Tinkler editors). AGU vol. 106, American Geophysical Union, Washington, D.C.

Peterson, L.C., Haug, G.H., Hughen, K.A. and Rohl, U. (2000) Rapid changes in the hydrologic cycle of the tropical Atlantic during the last glacial. *Science*, **290**, 1947–1951.

Prospero, J.M. (1996) Saharan dust transport over the North Atlantic Ocean and Mediterranean: an overview. Pp. 133–151 in: *The Impact of Desert Dust Across the Mediterranean* (S. Guerzoni and R. Chester, editors). Kluwer Academic Publishing, Dordrecht, The Netherlands.

Prospero, J.M., Glaccum, R.A. and Nees, R.T. (1981) Atmospheric transport of soil dust from Africa to South America. *Nature*, **289**, 570–572.

Reynolds, R.C., Jr. and Reynolds, R.C., III (1997) NEWMOD-for-Windows©: A computer program for the calculation of one-dimensional diffraction patterns of mixed-layered clays. Published by the authors, Hanover, New Hampshire, USA.

Righi, D., Terribile, F. and Petit, S. (1998) Pedogenic formation of high-charge beidellite in a vertisol of Sardinia (Italy). *Clays and Clay Minerals*, **46**, 167–177.

Righi, D., Terribile, F. and Petit, S. (1999) Pedogenic formation of kaolinite-smectite mixed-layers in a soil toposequence developed from basaltic parent material in Sardinia (Italy). *Clays and Clay Minerals*, **47**, 505–514.

Sak, P.B., Fisher, D.M., Gardner, T.W., Murphy, K. and Brantley, S.L. (2004a) Rates of weathering rind formation on Costa Rican basalt. *Geochimica et Cosmochimica Acta*, **68**, 1453–1472.

Sak, P.B., Fisher, D.M. and Gardner, T.W. (2004b) Effects of subducting seafloor roughness on upper plate vertical tectonism: Osa Peninsula, Costa Rica. *Tectonics*, **23**, TC1017, doi: 10.1029/2002TC001474.

Silver, E., Pisani, P.C., Hutnak, M., Fisher, A., DeShon, H. and Taylor, B. (2004) An 8–10 Ma tectonic event on the Cocos

Plate offshore Costa Rica: Result of Cocos Ridge collision? *Geophysical Research Letters*, **31(18)**: Art. No. L18601

Singh, B. and Gilkes, R.J. (1992) An electron-optical investigation of the alteration of kaolinite to halloysite. *Clays and Clay Minerals*, **40**, 212–229.

Środoń, J., Drits, V.A., McCarty, D.K., Hsieh, J.C.C. and Eberl, D.D. (2001) Quantitative X-ray diffraction of clay-bearing rocks from random preparations. *Clays and Clay Minerals*, **49**, 514–528.

Takahashi, T., Dahlgren, R. and van Susteren, P. (1993) Clay mineralogy and chemistry of soils formed in volcanic materials in the xeric moisture regime of Northern California. *Geoderma*, **59**, 131–150.

Vidic, N.J. and Lobnik, F. (1997) Rates of soil development of the chronosequence in the Ljubljana basin, Slovenia. *Geoderma*, **76**, 35–64.

White, A.F., Blum, A.E., Schulz, M.S., Vivit, D.V., Stonestrom, D.A., Larsen, M., Murphy, S.F. and Eberl, D.D. (1998) Chemical weathering in a tropical watershed, Loquillo Mountains, Puerto Rico: I. Long-term versus short-term weathering fluxes. *Geochimica et Cosmochimica Acta*, **62**, 209–226.

Wilson, M.J. and Cradwick, P.D. (1972) Occurrence of interstratified kaolinite-montmorillonite in some Scottish soils. *Clay Minerals*, **9**, 435–437.

Yerima, B.P.K., Calhoun, F.G., Senkayi, A.L. and Dixon, J.B. (1985) Occurrence of interstratified kaolinite-smectite in El Salvador vertisols. *Soil Science Society of America Journal*, **49**, 462–466.

(*Received 7 October 2005; revised 3 April 2006; Ms. 1045*)